Highly Sensitive Defect Detectors and Comparators Exploiting Port Imbalance in Rat-Race Couplers Loaded With Step-Impedance Open-Ended Transmission Lines

Cristian Herrojo, *Member, IEEE*, Paris Vélez, *Senior Member, IEEE*, Jonathan Muñoz-Enano, *Student Member, IEEE*, Lijuan Su, *Member, IEEE*, Pau Casacuberta, Marta Gil, and Ferran Martín, *Fellow, IEEE*

Abstract— Defect detectors and comparators, able to detect tiny differences between a reference (REF) sample and a material under test (MUT), are presented in this paper. In one version, the comparator is implemented by means of a rat-race hybrid coupler and a single step-impedance open-ended transmission line connected to one of the ports of the coupler. The comparator exploits the imbalance generated in one of the two pairs of isolated ports of the coupler when the MUT sample differs from the REF sample. The other pair of isolated ports is used for comparator feeding (Δ-port) and for recording the output signal (Σ-port), and feeding is achieved by means of a harmonic signal tuned to the operating frequency of the coupler. The resulting device is therefore a two-port structure, and the considered output variable is the magnitude of the transmission coefficient, an easily measurable quantity. By virtue of the step-impedance transmission line, used as the sensitive element of the comparator, the device exhibits very high sensitivity to variations in the dielectric constant between the REF and MUT samples, this being the input variable. A prototype device example, with a maximum sensitivity of 0.72 is reported, and applied to the detection of defects in the REF sample, a dielectric slab, generated by drilling holes of different densities across it. In the second prototype, a true differential-mode sensor, two identical sensing elements (step impedance lines) are connected to one of the pairs of isolated ports of the coupler, and roughly perfect balance is obtained when the MUT is identical to the reference sample. The maximum sensitivity in this case is 1.20, and the device discriminates also small perturbations generated in the REF material. The main relevant aspect of the reported prototypes, phase-variation sensing devices by nature, is the phase-to-magnitude conversion achieved by means of the hybrid coupler. This transforms the reflective-mode phase-variation sensing element to a two-port transmission-mode device where the output variable is the magnitude of the transmission coefficient, an easily measurable quantity.

Index Terms— Comparator, defect detector, dielectric constant sensor, microwave sensor, microstrip technology, phase-variation sensor, rat-race coupler, step-impedance transmission line.
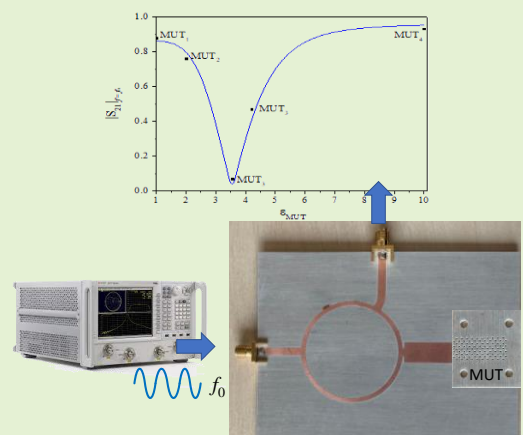
I. INTRODUCTION

MICROWAVE COMPARATORS are sensing devices focused on identifying potential differences between a well-known sample (usually designated as reference –REF– sample) and the so-called sample, or material, under test (MUT) using microwave signals. Typically, although not exclusively, the comparator functionality is based on detecting variations in the dielectric constant (or effective dielectric constant) of the MUT with regard to the one of the REF sample. Such microwave comparators can therefore be implemented by means of differential, or quasi-differential, dielectric constant sensors, where the input signal is the differential dielectric constant between the REF and the MUT sample. Such differential-mode

devices are robust against cross sensitivities, e.g., caused by changes in environmental factors (temperature or humidity), or noise, and are of special interest for real-time monitoring potential changes in the MUT. However, differential or quasi-differential sensors require two sensing elements and, consequently, such sensors typically exhibit larger dimensions than their single-ended counterparts. Nevertheless, there are applications where the cited advantages of differential sensing are not needed. In these cases, comparators based on (smaller) single-ended sensors suffice, but, obviously, at the cost of performing the measurements in a two-step process (first, the response of the REF sample is inferred, and then the one of the MUT is obtained).

There are various approaches for the implementation of dielectric constant microwave sensors/comparators, including frequency variation [1]-[20], coupling modulation [21], phase variation [22]-[32], frequency splitting [33]-[43], and, obviously, a combination of the previous approaches. Frequency splitting sensors are, by nature, quasi-differential devices where two resonators are used for sensing. In such sensors, the comparator functionality is based on the splitting in frequency of the (typically) notched response, caused by symmetry disruption (e.g., generated by differences between the REF and MUT samples). Nevertheless, frequency-splitting sensors implemented by means of bandpass structures have also been reported [39]. Comparators implemented by means of frequency-splitting sensors, applied to the detection of defects in samples, have been reported [37],[42],[43]. The other sensor types can be implemented, in general, as single-ended or as differential-mode structures. For example, differential-mode phase-variation sensors useful as comparators have been presented in [24],[44]. Other differential-mode sensors devoted to material characterization are reported in [45]-[54].

In comparators, the key parameter is the resolution, since it determines the capacity of the device to discriminate small differences between the REF and the MUT samples. The resolution is given by the minimum detectable value of the input variable, and it is intimately related to the sensitivity at small perturbations. Thus, high-resolution comparators should be necessarily implemented by means of highly-sensitive sensors. Sensitivity enhancement combined with small sized sensors is probably the most challenging issue for microwave engineers working on sensor's research and development. In this regard, it has been recently demonstrated that a kind of phase-variation sensors, operating in reflective mode, exhibit unprecedented sensitivities with a limited size of the sensing area, provided they are adequately designed [26]-[29]. These sensors consist of either a low-impedance half-wavelength or a high-impedance quarter-wavelength open-ended sensing line cascaded to a set of high/low impedance quarter-wavelength transmission line sections (impedance inverters). The impedance contrast of the inverters generates a multiplicative effect on the sensitivity of these step-impedance transmission line based sensors, and sensitivities as high as 528.7° in sensors devoted to the determination of the dielectric constant of the MUT (the input variable) have been obtained [26].

In this paper, microwave comparators based on these highly-sensitive reflective-mode phase-variation sensors are reported. By using a rat-race hybrid coupler with the step-impedance open-ended sensing lines connected to two of the isolated ports, the phase information is converted to magnitude information. The resulting overall devices are two-port structures where the output variable is the magnitude of the transmission coefficient, whereas the input variable is the differential dielectric constant between the REF and the MUT samples. With the proposed configuration, any imbalance between the reflection coefficients seen from the isolated ports of the coupler, caused by a difference between the REF and the MUT samples, is detected by a finite transmission coefficient (ideally null under perfect balance). The use of the imbalance in the rat-race coupler combined with the use of impedance-contrast step-impedance sensing arms is the main novel aspect of the paper. A detailed sensitivity analysis is carried out, and the effects of losses are also discussed.

The paper is organized as follows. Section II presents the proposed comparators as well as their working principle. A sensitivity analysis is reported, and validated through simulation, in Section III. Section IV is focused on the experimental validation. Two prototype comparators, designed according to the guidelines of Section III, have been fabricated, and their functionality is demonstrated by comparing the REF sample with several defected samples, inferred from the REF sample by drilling arrays of holes of different densities, and several MUTs. A comparison to other comparators is the subject of Section V. Finally, the main conclusions are highlighted in Section VI.

II. THE PROPOSED COMPARATOR AND WORKING PRINCIPLE

The proposed comparators consist of a reflective-mode differential phase-variation dielectric constant sensor connected to one of the pairs of the isolated ports of a rat-race hybrid coupler, as depicted in the schematic of Fig. 1. The resulting device is a two-port structure, where the input signal is injected to the Δ-port (port 1 in Fig. 1), whereas the output variable is recorded in the Σ-port (port 2 in Fig. 1). With this configuration, the differential phase of the reflection coefficients seen from the isolated ports of the coupler (the usual output variable in reflective-mode differential phase-variation sensors) is converted to magnitude information. The output variable in the proposed sensor/comparator is thus the magnitude of the transmission coefficient, which can be measured by means of a vector network analyzer (VNA). This approach has been carried out in this paper, as far as the main purpose is to validate these comparators by means of proof-of-concept demonstrators at laboratory level. Nevertheless, it is possible to replace the VNA with a microwave oscillator connected to the Δ-port and tuned to the operating frequency of the rat-race coupler, f_0, and an amplitude detector connected to the Σ-port. With this strategy, reported previously in various sensors proposed by the authors [21],[55]-[56], the output variable is the voltage amplitude of the harmonic signal generated in the output port of the structure, related to signal imbalances in the isolated ports of the coupler.
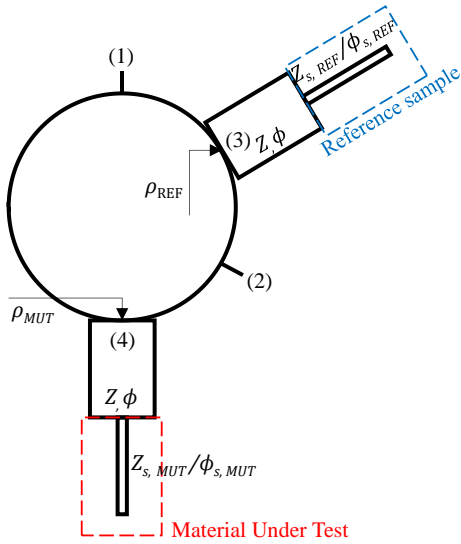
Fig. 1. Schematic of the proposed sensor/comparator with indication of the ports and the main relevant variables. The dashed rectangles indicate the sensing regions for the REF and MUT samples.

Let us designate by ρ_{REF} and ρ_{MUT} the reflection coefficients seen from port 3 and 4, respectively, of the coupler (where the REF and MUT step-impedance sensing lines are connected), see Fig. 1. By neglecting ohmic, dielectric and radiation losses, such reflections coefficients satisfy $|\rho_{REF}| = |\rho_{MUT}| = 1$, regardless of the loads present in the REF and MUT sensing lines. Thus, under this approximation, any potential imbalance between the isolated ports should be entirely due to a difference in the phase of the reflection coefficients, intimately related to changes in the MUT as compared to the REF sample. Since such phase imbalance between the isolated ports of the coupler provides a finite output signal in the Σ-port dependent on it (as it will be shown in the next section), it follows that the device is able to detect differences between the REF and the MUT samples. Note that the sensitive part of the device is the pair of open-ended sensing lines, with an electrical length (or phase) that depends on the dielectric constant of the material (REF or MUT material) on top of it. The cascaded 90º line sections with alternating high and low impedance generate a multiplicative effect on the phase of the reflection coefficient of the lines, as reported in [26], thereby enhancing the sensitivity. Note that in the schematic of Fig. 1, a single 90º line (with impedance Z and phase $\phi = 90º$ at f_0) cascaded to the open-ended sensing line is considered, in accordance with the prototypes of this work. However, further 90º stages, with alternating high and low impedance, can be introduced, as reported, e.g., in [26], in order to further boost up the sensitivity.

According to these words, it is clear that the comparator functionality relies in the capability of the device to measure the differential dielectric constant between the REF and MUT samples. Obviously, in order to implement a comparator with high discrimination capability, or resolution, it is necessary to achieve high sensitivity in the limit of small perturbations. This justifies the need to cascade the high/low impedance 90º lines between the sensing line and the isolated ports of the coupler.

III. SENSITIVITY ANALYSIS

Under the lossless approximation, the transmission coefficient between the input and the output port of the circuit of Fig. 1, S_{21}, can be expressed in terms of the phases of the reflection coefficients seen from the isolated ports, ϕ_{REF} and ϕ_{MUT}, as

$$S_{21} = -\frac{1}{2}\left(\rho_{REF} - \rho_{MUT}\right) = -\frac{1}{2}\left(e^{j\phi_{REF}} - e^{j\phi_{MUT}}\right) \quad (1)$$

The magnitude of the transmission coefficient can be easily calculated, i.e.,

$$|S_{21}| = \frac{1}{2}\sqrt{2\left(1 - \cos\Delta\phi_\rho\right)} \quad (2)$$

where $\Delta\phi_\rho = \phi_{REF} - \phi_{MUT}$ is the differential phase of the reflection coefficients. Note that for identical REF and MUT samples $|S_{21}| = 0$ (since $\Delta\phi_\rho = 0$), whereas the output variable is a maximum ($|S_{21}| = 1$) for a combination of REF and MUT samples providing out-of-phase reflection coefficients (with $\Delta\phi_\rho = \pi$, or $\rho_{REF} = -\rho_{MUT}$).

The sensitivity, or derivative of the output variable, $|S_{21}|$, with the input variable, i.e., the differential dielectric constant, $\Delta\varepsilon = \varepsilon_{REF} - \varepsilon_{MUT}$, can be expressed as

$$S = \frac{d|S_{21}|}{d\Delta\varepsilon} = \frac{d|S_{21}|}{d\Delta\phi_\rho} \cdot \left\{\frac{d\Delta\phi_\rho}{d\Delta\phi_s} \cdot \frac{d\Delta\phi_s}{d\Delta\varepsilon} + \frac{d\Delta\phi_\rho}{d\Delta Z_s} \cdot \frac{d\Delta Z_s}{d\Delta\varepsilon}\right\} \quad (3)$$

with $\Delta\phi_s = \phi_{s,REF} - \phi_{s,MUT}$, $\phi_{s,REF}$ and $\phi_{s,MUT}$ being the electrical lengths of the sensing line sections for the REF and MUT lines, respectively, and $\Delta Z_s = Z_{s,REF} - Z_{s,MUT}$, where $Z_{s,REF}$ and $Z_{s,MUT}$ are the characteristic impedances of those sections. The first term of the right-hand side member in (3) is

$$\frac{d|S_{21}|}{d\Delta\phi_\rho} = \frac{\sin\Delta\phi_\rho}{2\sqrt{2\left(1 - \cos\Delta\phi_\rho\right)}} \quad (4)$$

The derivatives $d\Delta\phi_\rho/d\Delta\phi_s$ and $d\Delta\phi_\rho/d\Delta Z_s$ depend on the electrical length of the sensing line. However, it was demonstrated in [26] that for sensitivity optimization in step-impedance open-ended sensing line based sensors in the vicinity of the REF dielectric constant (the one of the REF sample), the electrical length of the sensing line should not be arbitrary. Particularly, such electrical length (with the REF material on top of the sensing line) should be either $\phi_s = 90º$ (or odd multiples) or $\phi_s = 180º$ (or even or odd multiples). Moreover, for sensitivity optimization with the phase of the sensing line set to $\phi_s = 90º$, the characteristic impedance of such line must be high, whereas the impedance of the cascaded 90º line sections (if they are present) must alternately be low and high. Additionally, the impedance of the 90º line section adjacent to the sensing line must be low. By contrast, for sensitivity optimization with the phase of the sensing line set to $\phi_s = 180º$, the impedance of such line must be low, whereas the impedance of the adjacent 90º line sections must be high, and, if there are further sections, their impedance value must be alternately low and high.

It was also demonstrated in [26] that for the phases that

optimize the sensitivity, $\phi_s = 90°$ or $\phi_s = 180°$, the derivative $d\Delta\phi_\rho/d\Delta Z_s$ in the limit of small perturbations is null. Thus, the second summand of the right-hand side member in (3) can be neglected in that limit. It should be mentioned that for comparator functionality, the main interest is the optimization of the sensitivity for small imbalances, or for small variations of the dielectric constant of the MUT with regard to the one of the REF material. The reason is that sensitivity optimization in the vicinity of the REF dielectric constant improves the resolution of the comparator.

In order to calculate the sensitivity for low perturbations, the two cases corresponding to the two optimum phases of the open-ended sensing line should be analyzed separately. Thus, for $\phi_s = 180°$, the sensitivity of the differential phase of the reflection coefficients with the differential phase of the lines is [26]

$$\frac{d\Delta\phi_\rho}{d\Delta\phi_s} = \frac{-2Z^2}{Z_0 Z_s} = -2\frac{\bar{Z}^2}{\bar{Z}_s} \qquad (5a)$$

whereas for $\phi_s = 90°$, the following result was obtained

$$\frac{d\Delta\phi_\rho}{d\Delta\phi_s} = \frac{-2Z_0 Z_s}{Z^2} = -2\frac{\bar{Z}_s}{\bar{Z}^2} \qquad (5b)$$

where Z_0 is the reference impedance of the ports, Z_s is the nominal impedance of the sensing lines, i.e., $Z_s = Z_{s,REF}$, and Z is the characteristic impedance of the 90° line section cascaded to the sensing line (a single 90° line section, plus the sensing line section, is considered in this paper). In addition, the normalized impedances $\bar{Z}_s = Z_s/Z_0$ and $\bar{Z} = Z/Z_0$ have been used in (5). From (5), it is clear that for sensitivity optimization, the impedances must satisfy $Z_s > Z_0 > Z$ for $\phi_s = 90°$, and $Z_s < Z_0 < Z$ for $\phi_s = 180°$, as anticipated before. Finally, the sensitivity of the differential phase of the sensing lines with the differential dielectric constant is [26]

$$\frac{d\Delta\phi_s}{d\Delta\varepsilon} = \frac{\phi_{s,REF}}{4\varepsilon_{eff}}(1 - F) \qquad (6)$$

where sensor implementation in microstrip technology has been considered. In (6), ε_{eff} is the effective dielectric constant of the MUT open-ended sensing line, i.e. [57],

$$\varepsilon_{eff} = \frac{\varepsilon_r + \varepsilon_{MUT}}{2} + \frac{\varepsilon_r - \varepsilon_{MUT}}{2}F \qquad (7)$$

where ε_r is the substrate dielectric constant, and F is a geometry factor given by

$$F = \left(1 + 12\frac{h}{W_s}\right)^{-\frac{1}{2}} \qquad (8a)$$

for $W_s/h \geq 1$, or by

$$F = \left(1 + 12\frac{h}{W_s}\right)^{-\frac{1}{2}} + 0.04\left(1 - \frac{W_s}{h}\right)^2 \qquad (8b)$$

for $W_s/h < 1$, where h and W_s are the substrate thickness and the width of the MUT sensing line, respectively, and it is assumed that $t << h$, where t is the thickness of the metallic layer. Note that the validity of (7) is subjected to the semi-infinite MUT approximation. That is, the MUT must be thick enough in the vertical direction, so that the electromagnetic field generated by the line does not reach the MUT-air interface.

In the limit of small perturbations (with $\Delta\varepsilon \to 0$, and, consequently, $\Delta\phi_\rho \to 0$), the contribution to the sensitivity given by (4) is simplified to

$$\frac{d|S_{21}|}{d\Delta\phi_\rho} = \frac{1}{2} \qquad (9)$$

where the L'Hôpital rule has been applied to expression (4) in order to solve the indeterminacy in the considered limit. Therefore, using (5), (6) and (9), the overall sensitivity in the vicinity of the dielectric constant of the REF material (low-perturbation) is found to be

$$S = \frac{d|S_{21}|}{d\Delta\varepsilon} = -\frac{\bar{Z}^2}{\bar{Z}_s}\frac{\pi}{4\varepsilon_{eff}}(1 - F) \qquad (10a)$$

for the sensors based on 180° sensing lines, and

$$S = \frac{d|S_{21}|}{d\Delta\varepsilon} = -\frac{\bar{Z}_s}{\bar{Z}^2}\frac{\pi}{8\varepsilon_{eff}}(1 - F) \qquad (10b)$$

for the sensors implemented by means of 90° sensing lines.

Let us next validate the previous sensitivity analysis at schematic level, where losses, as well as other potential non-ideality effects, are ignored. For that purpose, let us consider that the frequency of operation is set to $f_0 = 2$ GHz. The considered substrate has the characteristics of the *RO4003C* substrate with thickness $h = 1.52$ mm and dielectric constant $\varepsilon_r = 3.55$. Nevertheless, for the purpose of validation of the previous analysis, let us consider ideal components, except the open-ended sensing line section, subjected to the presence of a MUT on top of it. Thus, the impedance of the line sections of the coupler (with a total ring length of 1.5λ, or an electrical length of 540°) is 70.71 Ω, i.e., the necessary value to obtain a –3dB hybrid coupler by considering a port impedance of $Z_0 = 50$ Ω. Concerning the loads seen from the isolated ports of the coupler, namely, the step-impedance lines, we have considered sensing lines with phase and impedance of $\phi_s = 90°$ and $Z_s = 131$ Ω, respectively, when they are covered by a semi-infinite material with dielectric constant $\varepsilon_{REF} = 3.55$ (corresponding to one of the low-loss microwave substrates available in our laboratory), the REF dielectric constant. Between the open-ended sensing lines and the respective ports of the coupler, a low-impedance 90° line section with $Z = 29$ Ω, is inserted. Such line sections (one for each isolated port of the coupler) are considered to be ideal. However, for the sensing lines, it is necessary to consider "real components", subjected to the presence of a material (REF or MUT sample) on top of it. Indeed, the *Keysight ADS* schematic simulator provides a component consisting of a transmission line section including the presence of a dielectric layer on top of it, in our case the REF and the MUT samples. With the considered substrate and with a semi-infinite material of $\varepsilon_{REF} = 3.55$ on top of the sensing line, the physical length and width of such line, providing the above-cited phase and impedance values, are 19.89 mm and 0.20 mm, respectively (actually, the impedance Z_s was set to the value providing the minimum achievable width with the available fabrication technology).
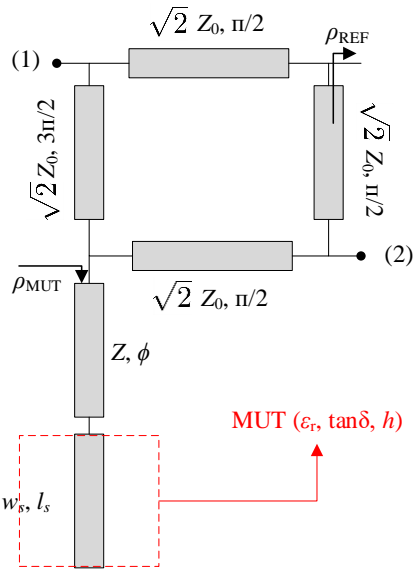
Fig. 2. Schematic used for the simulations devoted to the validation of the sensitivity analysis.
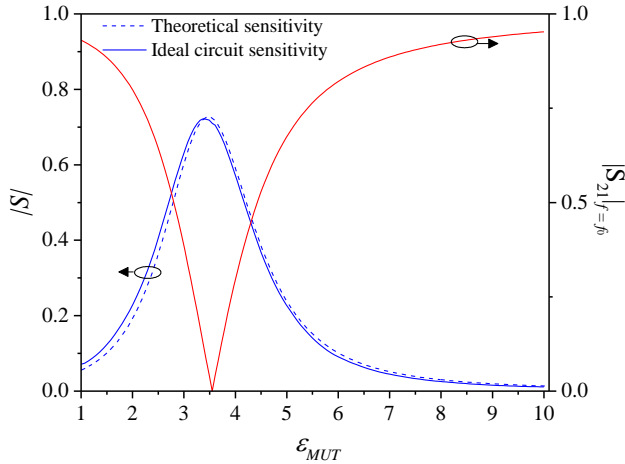

Fig. 3. Sensor/comparator response corresponding to the schematic of Fig. 2, inferred from circuit simulation, and sensitivity.
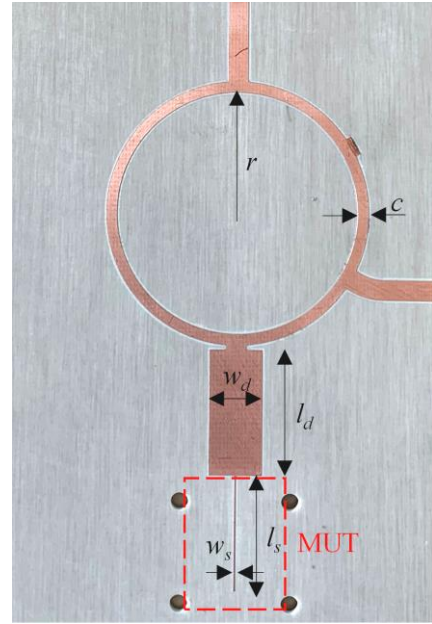

Fig. 4. Photograph of the sensor/comparator based on a single sensing line. The sensing region is indicated by a dashed rectangle. Dimensions are (in mm): $w_s = 0.20$, $l_s = 19.89$, $w_d = 9.07$, $l_d = 21.05$, $c = 1.88$, $r = 21.15$.

the simulated data points (the results are also included in the figure). The absolute value of the sensitivity in the limit of small perturbations, i.e., for $\Delta\varepsilon = 0$ (or $\varepsilon_{REF} = \varepsilon_{MUT}$), inferred from the simulated data, is found to be 0.722 whereas the one predicted by the theory, by means of (10b), is 0.727, that is, in very good agreement with the simulated value. Therefore, with this study, based on schematic simulations, the sensitivity analysis is validated. It is important to mention that there are two values of the dielectric constant of the MUT which provides the same value of the magnitude of the transmission coefficient. In order to discriminate the correct value of the dielectric constant, the phase of the transmission coefficient must be obtained. The different sign of the phase at both sides of ε_{REF}, as it can be easily inferred from (1), allows us to distinguish whether $\varepsilon_{MUT} < \varepsilon_{REF}$ or $\varepsilon_{MUT} > \varepsilon_{REF}$.

Note that the sensitivity is dimensionless since it involves dimensionless input and output variables. It should also be mentioned that in a real sensor, the effects of losses, including (potential) radiation losses, might alter the impedance seen from the isolated ports of the coupler, when the corresponding sensing line is covered by the REF material. This may result in signal imbalance when the MUT coincides with the REF sample, provided one of the isolated ports is left opened (as in Fig. 2), thereby generating sensitivity degradation. Nevertheless, this aspect, related to the effects of losses, will be discussed in the next section and in Appendix A.

IV. SENSOR/COMPARATOR DESIGN, FABRICATION, AND EXPERIMENTAL VALIDATION

We have designed and fabricated two prototype sensor/comparators. One of them corresponds to the schematic of Fig. 2, and is used to check the validity of performing

Once the simulation conditions have been established, the next step is to obtain the sensor/comparator response, i.e., the magnitude of the transmission coefficient at f_0 as a function of the differential dielectric constant. Nevertheless, a simplification can be made, since the reflection coefficient of the REF step-impedance line does not change. Indeed, such reflection coefficient is $\rho_{REF} = 1$, as explained by the fact that the impedance seen from that port is infinite. The reason is that the pair of cascaded 90º lines translate the termination impedance (an open-circuit) to the coupler port. Thus, if the frequency is kept to f_0, no changes are expected in the sensor/comparator response if the port (3) of the coupler is left opened.

With the above-mentioned simplification, the schematic of the simulated structure is the one depicted in Fig. 2. Figure 3 depicts the dependence of $|S_{21}|$ with ε_{MUT} (at f_0) obtained by means of the schematic simulator of *Keysight ADS*. From this curve, the sensitivity has been inferred by simple derivation of
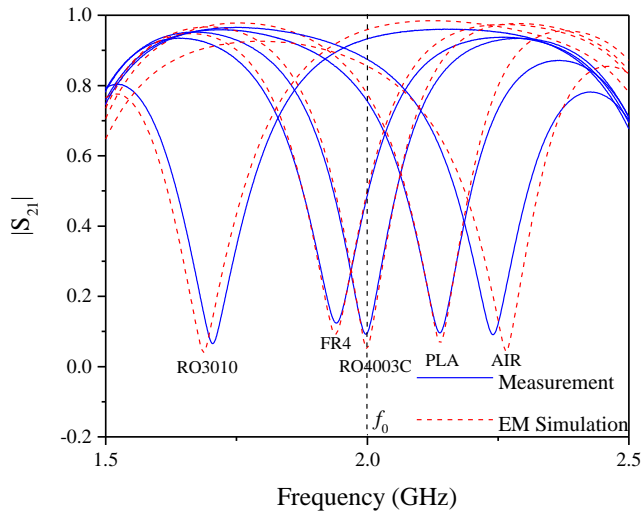
Fig. 5. Frequency response of the sensor comparator of Fig. 4 for different MUT samples placed in the sensing region. The dielectric constants of the MUTs are: for *RO4003C*, the REF sample, $\varepsilon_{MUT} = \varepsilon_{REF} = 3.55$, for RO3010, $\varepsilon_{MUT} = 10.2$, for FR4, $\varepsilon_{MUT} = 4.4$, for PLA, $\varepsilon_{MUT} = 2$, and for air, $\varepsilon_{MUT} = 1$.
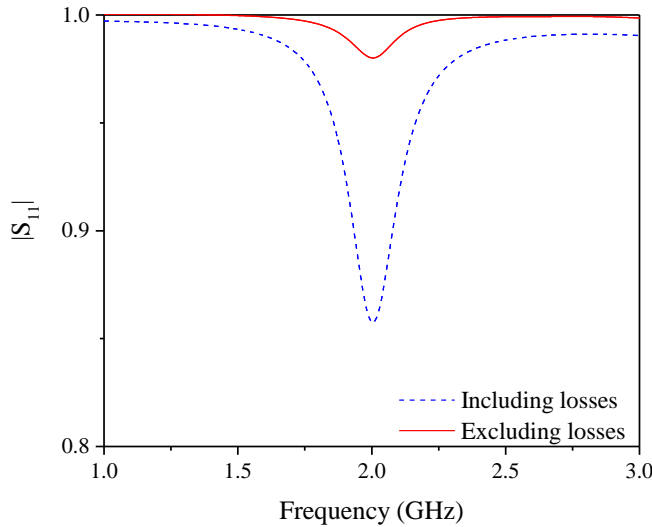

Fig. 6. Simulated reflection coefficient of the sensing line of Fig. 4 (together with the cascaded 90º line section) by including and by excluding ohmic and dielectric losses.

comparisons in a two-step process, as indicated before, with the advantage of a simpler structure, where one of the step-impedance lines, the one devoted to the REF sample, is replaced with an open circuit. The second prototype is a true differential sensor/comparator where both sensing lines are included in the design. In this second prototype, the sensing lines are low-impedance half-wavelength open-ended lines.

A. Prototype sensor/comparator with a single sensing line (Sensor A)

The structure corresponding to the schematic of Fig. 2 was fabricated by means of the *LPKF H100* drilling machine on the low-loss microwave substrate indicated in the previous section (with thickness $h = 1.52$ mm, dielectric constant $\varepsilon_r = 3.55$ and loss tangent $\tan\delta = 0.0021$). The photograph of the device is depicted in Fig. 4. Figure 5 depicts the frequency responses for
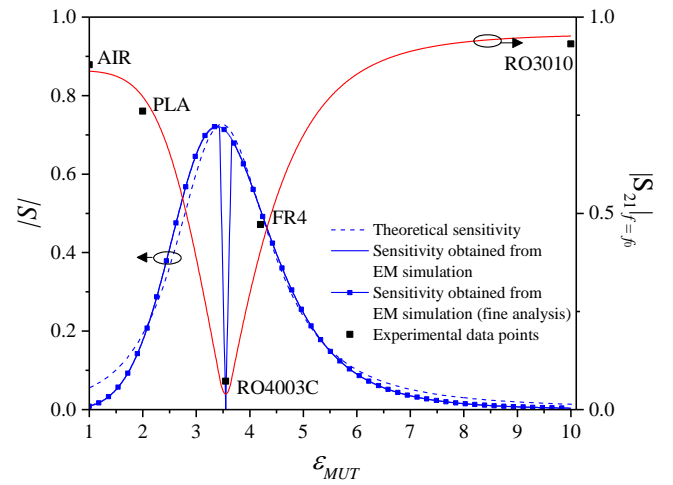

Fig. 7. Sensor/comparator response and sensitivity corresponding to the device of Fig. 4. The experimental data points are included in the figure.

different values of the dielectric constant of the MUT, corresponding to dielectric samples (uncladded microwave substrates in most cases) available in our laboratory. Actually, the figure includes the measured responses, inferred by means of the *Agilent N5221A* vector network analyzer, as well as the responses obtained by means of electromagnetic simulation, using the *ANSYS HFSS* electromagnetic solver. The thickness of the samples is 3 mm, reasonably thick to consider them semi-infinite in the vertical direction. The potential effects of air gap between the MUT and the sensing region have been minimized by adding pressure on the MUT sample against the sensor substrate. It should also be mentioned that small lateral shifts in the MUT are not relevant as far as the transverse dimensions of the MUT extend significantly beyond the limits of the sensing line. According to these comments, as far as the semi-infinite approximation in the MUT is satisfied in both the vertical and transverse dimensions, the size of the sample is irrelevant.

As it can be appreciated in Fig. 5, for an MUT identical to the REF sample (*RO4003C* with $\varepsilon_{MUT} = \varepsilon_{REF} = 3.55$), the frequency response exhibits a transmission zero (partly obscured by losses) at $f_0 = 2$ GHz, indicative of a good balance between the loads seen from the isolated ports of the coupler (ports 3 and 4). Despite the fact that in port (3), there is a "real" open circuit, the virtual open circuit at port (4) when the MUT is the REF sample is quite satisfactory. To gain insight on this aspect, we have inferred the simulated reflection coefficient of the sensing line (including the cascaded 90º line section), with the REF material on top of the sensing region, see Fig. 6. Actually, we have performed two different simulations, i.e., in one case by excluding dielectric and ohmic losses, and in the other case by including them. The simulation by excluding ohmic and dielectric losses reveals that radiation losses are very small. The modulus of the reflection coefficient at f_0 is close to unity (0.86), when the ohmic and dielectric losses are included, but the effect of losses cannot be considered to be negligible. Nevertheless, the effects of losses on the sensitivity analysis carried out before are, apparently, irrelevant. To gain insight on this, Fig. 7 depicts the sensor/comparator response, i.e., the

magnitude of the transmission coefficient at f_0 as a function of the dielectric constant of the MUT. The figure includes simulated values (inferred by means of *ANSYS HFSS*), as well as the measured results directly translated from Fig. 5. The figure includes also the absolute value of the sensitivity, inferred from the simulated data points, where it can be appreciated that it exhibits a maximum at $\varepsilon_{MUT} = \varepsilon_{REF} = 3.55$, and the value of the maximum sensitivity is $|S|_{max} = 0.715$, in very good agreement with the prediction of the theory (0.727). Moreover, the agreement between the theoretical sensitivity and the values inferred from the simulated data points, in the considered range of ε_{MUT} variation, is very good, as revealed by Fig. 7.

Nevertheless, a fine analysis of the sensitivity in the vicinity of the reference value of the dielectric constant of the MUT, reveals that the sensitivity exhibits a different behaviour at this limit. For that purpose, we have inferred the magnitude of the transmission coefficient for varying values of ε_{MUT} in the range 3.4–3.6, and the resulting sensitivity is also depicted in Fig. 7. Clearly, there is a minimum at $\varepsilon_{MUT} = \varepsilon_{REF}$ with a continuously varying slope. Consequently, the sensitivity should be null at this value of the dielectric constant of the MUT, the reference value. This effect is clearly related to losses, since, if losses are absent, there is a minimum at ε_{MUT}, but the absolute value of the derivative is finite (not null) and should coincide with the theoretical value, as indeed occurs, provided the derivative, i.e., the sensitivity, is inferred by considering a more sparse density of data points around the reference dielectric constant. According to these results, the theoretical expression of the sensitivity inferred by neglecting losses is not able to predict the null value of it for $\varepsilon_{MUT} = \varepsilon_{REF}$ when losses cannot be neglected. Appendix A includes the analysis when losses in the structure (sensing line) are present. From this analysis, it is concluded that when losses are present, the sensitivity in the limit when $\varepsilon_{MUT} = \varepsilon_{REF}$ is null, but the deviation from the theoretical value predicted in the analysis of the previous section is restricted to a narrow range of values in the vicinity of ε_{REF}. Moreover, in the limit when losses are null, the dip in the sensitivity disappears and the theoretical prediction given by (3), with (4), (5) and (6), is satisfied.

In summary, when the MUT is the REF sample, the measured transmission coefficient at f_0 is not exactly null. This is explained by the imperfect balance, due to the fact that one of the ports of the coupler is left open, whereas in the other port the losses (though small) prevent from the presence of a true open-circuit seen from that port. This effect drastically reduces the sensitivity as compared to the (lossless) theoretical value, but only in a very narrow region in the vicinity of ε_{REF}. This may have impact on the resolution, or capability to detect extremely small variations of the dielectric constant as compared to the REF value. Nevertheless, the sensitivity when the dielectric constant of the MUT is slightly different than ε_{REF}, coincides with the lossless prediction to a very good approximation, and the reason is that losses at f_0 progressively decrease when ε_{MUT} separates from ε_{REF}.

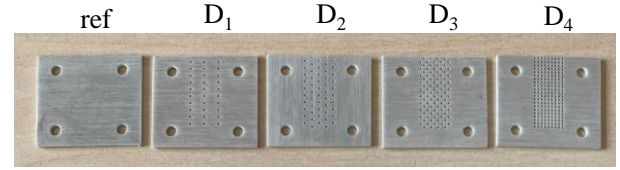The results reported so far confirm that it is licit to simplify

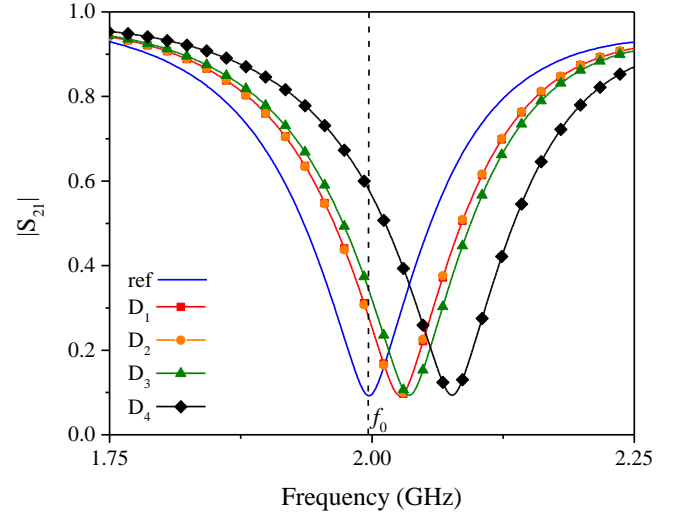Fig. 8. Defected samples obtained by drilling holes of different densities to the REF sample.

Fig. 9. Frequency response of the sensor/comparator of Fig. 4 for the different MUT samples of Fig. 8.

the structure by eliminating the sensing line devoted to the REF material, with the caution of the alteration of the sensitivity in the limit of small perturbations, which may prevent from the detection of tiny defects in samples (as compared to a reference sample). Nevertheless, real-time comparisons are not possible with this approach, as anticipated before. In order to demonstrate the potential of the sensor/comparator to discriminate changes in the MUT with regard to the REF sample, we have drilled arrays of holes of different densities across the REF samples, as depicted in Fig. 8. The measured frequency responses are shown in Fig. 9. The responses shift upwards as the density of holes increases because this decreases the "effective" dielectric constant of the samples. The sensor/comparator is able to detect the presence of holes in sample D_1, the one with the smaller density of holes. However, the response is identical to the one of sample D_2, and the reason is that the rows of holes at the sides of the central one (on top of the sensing line) are not under the influence of the electric field generated by the line, and, therefore, these samples are undistinguishable. Note, however, that for samples D_3 and D_4, the rows of holes are closer and the response varies. From the sensor/comparator transfer function of Fig. 7, an effective dielectric constant can be inferred for those drilled samples, but such effective dielectric constant does not have a physical meaning other than the necessary value of the dielectric constant of a hypothetical MUT to obtain the same magnitude of the transmission coefficient. Nevertheless, the comparator functionality is demonstrated, and the device is able to detect small imbalances between the REF and the MUT samples.
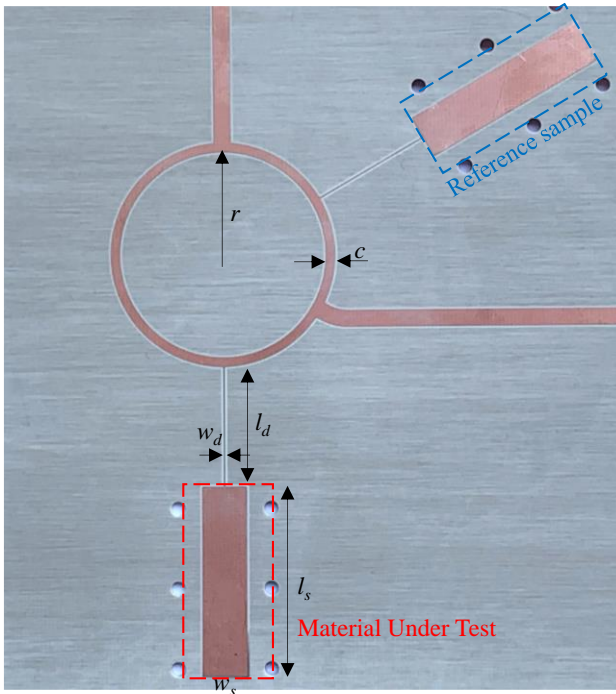
Fig. 10. Photograph of the sensor/comparator based on two sensing lines. The sensing regions, including the one devoted to the MUT and the one devoted to the REF sample, are indicated by dashed rectangles. Dimensions are (in mm): $w_s = 9.07$, $l_s = 39.81$, $w_d = 0.20$, $l_d = 24.65$, $c = 1.88$, $r = 21.15$.
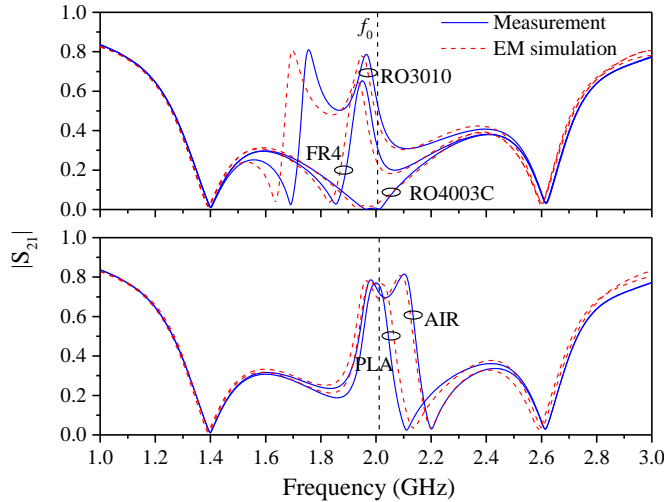

Fig. 11. Frequency response of the sensor comparator of Fig. 10 for different MUT samples placed in the sensing region, and the REF sample located on top of the REF line. The dielectric constants of the MUTs are: for *RO4003C*, the REF sample, $\varepsilon_{MUT} = \varepsilon_{REF} = 3.55$, for RO3010, $\varepsilon_{MUT} = 10.2$, for FR4, $\varepsilon_{MUT} = 4.4$, for PLA, $\varepsilon_{MUT} = 2$, and for air, $\varepsilon_{MUT} = 1$.

B. Prototype sensor/comparator with two sensing lines (Sensor B)

The second prototype is a true real-time differential sensor/comparator consisting of the rat-race hybrid coupler and two step-impedance sensing lines connected to the isolated ports. In this case, we have opted to implement the step-impedance lines by means of a low-impedance 180º open-ended sensing line cascaded to a high impedance 90º line. The
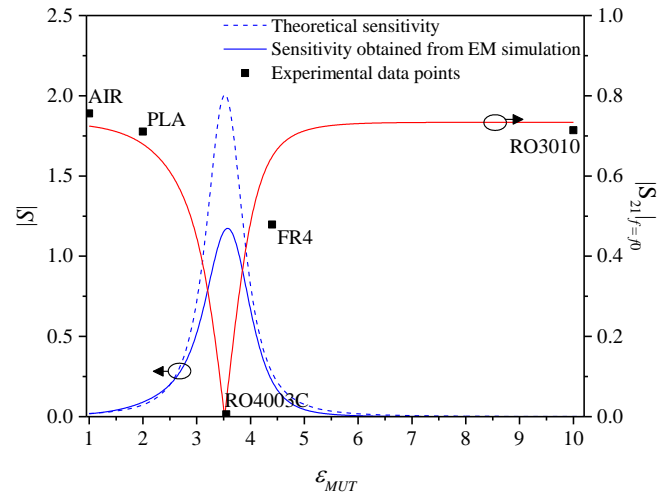
Fig. 12. Sensor/comparator response and sensitivity corresponding to the device of Fig. 10. The experimental data points are included.
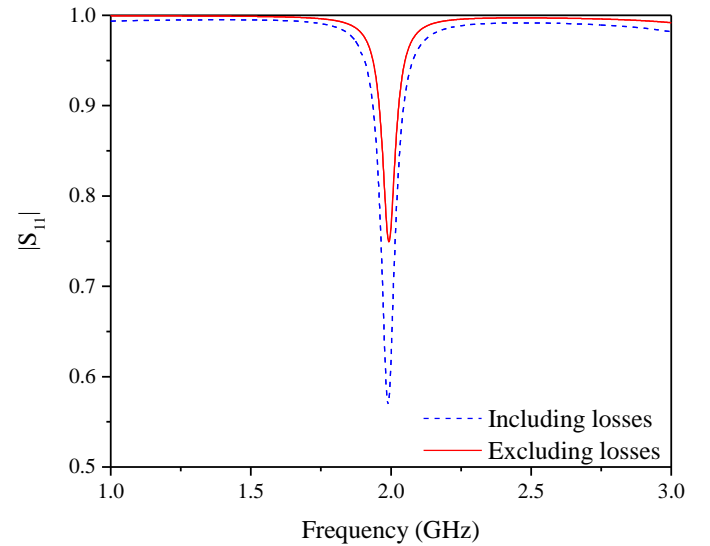
Fig. 13. Simulated reflection coefficient of the sensing line of Fig. 10 (together with the cascaded 90º line section) by including and by excluding ohmic and dielectric losses.

considered impedance values are $Z_s = 23\ \Omega$ and $Z = 157\ \Omega$. Obviously, the impedance and phase of the open-ended sensing line section is with the REF material (the same as in the previous prototype) on top of it. The sensor has been implemented on the same substrate used for the prototype of the preceding subsection, and the photograph of the fabricated device is depicted in Fig. 10, where dimensions are indicated.

The frequency responses inferred by loading the REF line with the REF material and the sensing line with different MUTs are depicted in Fig. 11, whereas Fig. 12 depicts the sensor/comparator response (transfer function), as well as the sensitivity (calculated from the simulated data points). It can be seen that the sensitivity differs significantly from the theoretical (lossless) value, also included in the figure. This difference is due to the effects of losses, not accounted for in the theoretical sensitivity analysis. Figure 13 depicts the simulated reflection coefficient of the sensing line (including the cascaded 90º line section), with the REF material on top of the sensing region. Analogously to Fig. 6, the figure depicts the reflection

Fig. 14. Frequency response of the sensor/comparator of Fig. 10 for the different MUT samples of Fig. 8.

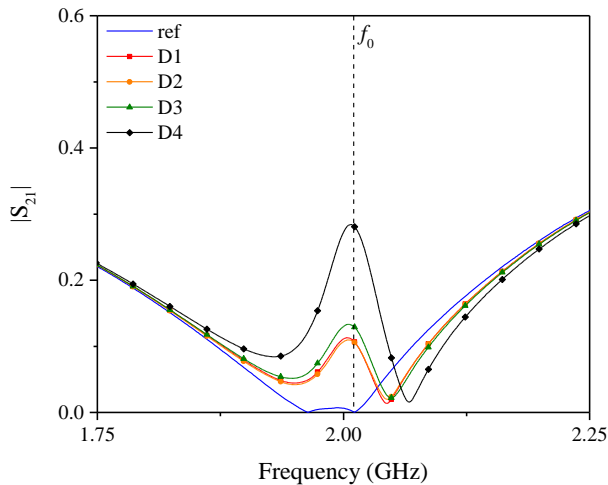coefficients by excluding and by including dielectric and ohmic losses. These results reveal that losses are significant (the modulus of the reflection coefficient at f_0 is 0.57) and that a significant portion of losses is due to radiation. However, since there is a quasi-perfect balance when the loads of the sensing lines are identical (the REF sample), the resulting transmission coefficient at f_0 is null to a very good approximation, as Fig. 11 reveals. Indeed, the loss level of $|\rho_{REF}|$ at f_0 for the sensing line loaded with the REF material can reasonably explain the difference in the sensitivity, at least in the limit of small perturbations. That is, if we assume that for MUTs with dielectric constants close to the one of the REF material the loss level at f_0 does not vary significantly (i.e., $|\rho_{MUT}| \approx |\rho_{REF}|$), expression (1) can be rewritten as

$$S_{21} = -\frac{1}{2}(\rho_{REF} - \rho_{MUT}) \approx -\frac{1}{2}|\rho_{REF}|(e^{j\phi_{REF}} - e^{j\phi_{MUT}}) \quad (11)$$

Under this approximation, the sensitivity analysis carried out in Section III is valid, with the exception of a multiplicative factor given by $|\rho_{REF}|$. Consequently, by correcting the lossless sensitivity ($|S| = 2.01$, see Fig. 12) taking into account the value of $|\rho_{REF}| = 0.57$, the resulting sensitivity in the limit of small perturbations should be reasonably predicted, as it actually occurs. Note that $|S| \cdot |\rho_{REF}| = 1.17$, whereas the sensitivity resulting from the simulated data points, obviously by including losses, is 1.18, i.e., in very good agreement. Losses tend to degrade the sensitivity, as it is clearly shown in this subsection. However, it does not mean that the sensor/comparator cannot be useful. Indeed, the results of Fig. 11 and 12 show the potential of the approach to determine the dielectric constant of the MUT from the measurement of the magnitude of the transmission coefficient. As comparator, by using two identical sensing arms, real-time differential measurements can be carried out by means of the device of Fig. 10. Moreover, the quasi-perfect balance, is beneficial in terms of resolution. The comparator functionality of the device of Fig. 10 has been demonstrated by obtaining the frequency responses corresponding to the defected REF samples of Fig. 8. The results are depicted in Fig. 14, and reveal the capability of the device to discriminate the differences with the REF sample,

even for the sample with a sparser hole density.

V. COMPARISON TO OTHER PHASE-VARIATION SENSORS

The main relevant advantage of the proposed sensor/comparator is the design simplicity combined with the fact that a differential measurement is implemented in a two-port device structure. An interesting, and competitive, approach was presented in [22], where a differential-mode dielectric constant sensor based on phase-variation and implemented by means of composite right/left-handed (CRLH) lines was reported. Such sensor operates in transmission, and the two-port configuration was achieved by feeding the differential port of the sensor with imbalanced signals generated by means of a balun, whilst the differential output port was connected to an identical balun in opposite configuration. The very high sensitivity of such sensor is due to the high dispersive behaviour of the CRLH lines [58]. In the sensors presented in this paper and that of [22], the phase information is converted to magnitude information. In [44], a two-port differential-mode phase-variation dielectric constant sensor operating in transmission was also reported. Phase-to-magnitude conversion was achieved in this case by means of a pair of rat-race hybrid couplers, and sensitivity was optimized by using meandered lines. The main advantage of the sensors of Figs. 4 and 10, as compared to the sensors in [22],[44], all of them differential and based on a two-port configuration, is the fact that in the sensors of this work the sensitivity can be enhanced without the need to increase the size of the sensing area (either a 90º or a 180º open-ended line section). For that purpose it suffices to add further quarter-wavelength transmission line sections with alternating high/low impedance. Obviously, this increases the overall size of the sensor, but not the sensing region. By contrast, in the sensors of [22],[44], the sensitivity is proportional to the length of the lines. Moreover, the sensors of this study are simply based on ordinary lines, thereby being robust against fabrication related tolerances or other detuning effects. Concerning the effects that additional quarter-wavelength line sections may produce on the sensor sensitivity through losses, it is expected that by considering low-loss microwave substrates, the case of the proposed sensors, such effects do not have significant influence on the sensor, provided the sensitivities are not extremely high. However, for highly sensitive sensors, losses degrade somehow the sensitivity as compared to the theoretical prediction by excluding losses (expressions 3 and 10). This aspect is analysed in further detail in the Appendix, where a method for the calculation of the sensitivity by considering the effects of losses is pointed out, and two additional illustrative examples of sensors (of type A) with enhanced sensitivity are reported.

In [25], differential sensors with very high sensitivity were reported, but at the expense of very long (meandered) lines, and hence large size of the sensing region. Moreover, these sensors are four-port structures. The sensors reported in [24] are also very interesting, as far as highly dispersive electro-inductive wave (EIW) artificial transmission lines are used for sensing. Such sensors exhibit very good sensitivity but are implemented

TABLE I
COMPARISON OF VARIOUS PHASE-VARIATION DIELECTRIC
CONSTANT SENSORS

Ref.	Mode*	Size (λ^2)	Max. Sensitivity	FoM ($^\circ/\lambda^2$)
[22]	TRANS-DIFF	---	600 dB	---
[23]	TRANS-SINGLE	---	54.8º	---
[25]	TRANS-DIFF	12.90	415.6º	32.2
[24]	TRANS-DIFF	0.075	25.3 dB	---
[44]	TRANS-DIFF	0.020	17.6 dB	---
[30]	TRANS-SINGLE	0.030	7.7º	257
[32]	TRANS-SINGLE	0.040	20.0º	500
[60]	TRANS-SINGLE	0.050	14.24º	284.8
[26]	REFLECT-SINGLE	0.025	528.7º	21148
[28]	REFLECT-SINGLE	0.100	45.5º	455
[29]	REFLECT-SINGLE	0.025	101.3º	4052
[52]	REFLECT-DIFF	0.003	1.6 dB/%	---
[A]	**REFLECT-DIFF**	**0.005**	**0.72/85.5º**	**16512**
[B]	**REFLECT-DIFF**	**0.062**	**1.17/230.6º**	**3671**

*TRANS-DIFF: transmission-mode differential; TRANS-SINGLE: transmission-mode single-ended; REFLECT-SINGLE: reflective-mode single-ended; REFLECT-DIFF: reflective-mode differential.

as four-port devices, and EIW lines are very sensitive to the effects of detuning and tolerances, since these artificial lines exhibit very narrow pass bands [59]. Note that the sensitivity in the sensors in [24] is given in dB. The reason is that the considered output variable is the cross-mode transmission coefficient, proportional to the difference in the transmission coefficients of the sensing EIW lines, intimately related to phase imbalance. Alternately, the sensitivity in such sensors can be expressed in linear form, as carried out in the present paper. Other differential sensors based on SRRs or CSRRs also use the cross-mode transmission coefficient as output variable [41],[47],[49], and exhibit good sensitivity, but such sensors need also four-port measurements.

As it has been reported in previous papers, the combination of sensitivity and size of the sensing region in reflective-mode phase-variation sensors implemented by means of step-impedance transmission lines is unique. The FoM, defined as the ratio between the maximum sensitivity and the size of the sensing region expressed in terms of the squared guided wavelength has unprecedented values in such sensors [26]-[29], as it can be seen in Table I (where several phase-variation sensors are compared). Note that the FoM is given only for those sensors where the output variable is the phase of either the transmission or the reflection coefficient. Nevertheless, the overall sensitivity of the sensors reported in this paper is entirely determined by the sensitivity of the step-impedance open-ended sensing line (the rat-race coupler mainly converts the phase to magnitude information, but does not contribute to boost up the sensitivity). These phase sensitivities are 85.5º and 230.6º for the sensors of Fig. 4 and 10, respectively, providing figures of merit of 16512º/λ^2 and 3671º/λ^2, and included in the table for comparison purposes. The maximum sensitivities that result by including the rat-race coupler and considering the magnitude of the transmission coefficient as output variable are $|S| = 0.72$ and $|S| = 1.17$ for the sensors of Fig. 4 and 10,

respectively.

Note that there are reflective-mode phase-variation sensors exhibiting an excellent figure of merit [26],[29]. The reason is that in such sensors, further high/low impedance quarter-wavelength line sections were included. The main purpose of this paper, rather than achieving an excellent sensitivity, has been to implement differential-mode structures based on two-port configurations, since it eases the measurements. Nevertheless, the reported sensitivities and FoM are good, and these parameters can be further enhanced by merely cascading additional quarter-wavelength line sections between the open-ended sensing line and the isolated ports of the coupler.

Note also that the phase-variation sensors presented in this work are differential-mode structures operating in reflection. There are other reflective-mode differential sensors reported in the literature [52], based on a topology similar to the sensor of Fig. 10. The sensing elements in this case are electrically small resonators, specifically open split ring resonators (OSRRs), but the design procedure was not carried out on the basis of the phase imbalance between the reflection coefficients seen from the isolated ports of the coupler. Indeed, the sensor of [52] was devoted to the characterization of liquids samples, particularly mixtures of isopropanol in deionized (DI) water, and for that reason that sensor was equipped with fluidic channels in the sensing regions. This sensor is included in Table I, but in this case the sensitivity is given in terms of dB/%, since the input variable is the volume fraction of isopropanol in DI water. Due to the high losses in liquid samples, port imbalance in the sensor of [52] is caused by changes in both the phase and the magnitude of the reflection coefficient seen from the ports. Nevertheless, the main dominant mechanism contributing to the output signal in this sensor is phase imbalance and, for this, reason, the device is also included in Table I. Moreover, it has been shown in the previous section that the effects of losses (despite the fact that the MUT are low-loss materials) cannot be neglected in the reported sensors.

Recently, single-ended phase-variation sensors operating in transmission and based on slow-wave transmission lines have been reported [30],[32]. Such sensors can be easily implemented as differential mode structures, and exhibit very reasonable FoM (especially the device in [32]), but their design is significantly more complex than the one of the sensors of this work.

Let us mention that at the expense of a more complex design, it is possible to replace the 90º or 180º open-ended sensing lines of the reported sensors with artificial lines (CRLH lines, slow-wave line, etc.). By this means, it is potentially possible to further enhance the sensitivity, yet keeping the size of the sensing region unaltered (or even reduced), due to the higher dispersion of artificial lines, as compared to ordinary lines. Nevertheless, this aspect requires further investigation and is left for future works.

Finally, to end this comparative analysis, let us emphasize that the reported sensors operate at a single frequency, in comparison to frequency-variation sensors, and this reduces the cost of the associated electronics in a real scenario, since wideband voltage controlled oscillators (VCOs) are not needed

in order to generate the interrogation signals of the sensors.

VI. Conclusions

In conclusion, microwave comparators based on reflective-mode differential phase-variation dielectric constant sensors have been reported in this paper. The devices are two-port structures consisting of a rat-race hybrid coupler with two of the isolated ports connected to the sensing elements, open-ended step-impedance transmission lines. The sensitivity of the sensors is high by virtue of the step-impedance configuration of the sensing lines, with a multiplicative effect caused by the step-impedance discontinuities. Two prototype sensor/comparators have been reported. In one case (sensor A), the sensing line devoted to the reference (REF) sample has been eliminated, in order to reduce the overall dimensions of the structure. This is justified because with the specific design, the impedance seen from the input port of the step-impedance REF sensing line is (ideally) an open-circuit. A comparison measurement with this device must be performed in a two-step process, where first the REF sample is measured, and then the response of the MUT is inferred. The second prototype (sensor B) is a real-time comparator with both sensing lines present (for the REF and MUT samples). Apart from this difference, the open-ended sensing line in sensor A is a high-impedance 90º line, whereas in sensor B, the sensitive element is a low-impedance 180º line. This combination of phase (either 90º or 180º) and impedance (either high or low) for the sensing lines obeys the design guidelines, inferred from the reported sensitivity analysis. Moreover, the 90º line section cascaded between the sensing line and the isolated ports of the coupler has been designed with the convenient impedance value (high or low), so as to boost up the sensitivity, also in coherence with the design guidelines. The sensitivities of the reported sensor/comparators are 0.72 and 1.17, dimensionless as far as the output variable is the magnitude of the transmission coefficient, the input variable being the differential dielectric constant between the REF and MUT samples. Nevertheless, these sensitivities can be expressed in terms of the equivalent phase sensitivity, in order to ease the comparison with other phase variation sensors (see Table I). The comparator functionality of both prototypes has been demonstrated by considering MUT samples consisting on pieces of the REF sample with sparse arrays of holes of different densities. Both devices are able to detect the samples with the smaller density of holes, thanks to the high sensitivity of the reported sensors. The effects of losses have also been analysed. It has been shown that in sensor A losses are low and have not a significant effect on the sensitivity, except for extremely small perturbations. For sensor B, device losses are more significant, and degrade the sensitivity as compared to the one predicted by the theory (where the effects of losses are excluded). Nevertheless, despite the higher level of losses, sensor B exhibits quasi-perfect balanced when the MUT sensing line is loaded with the REF sample, and, potentially, this sensor (with the pair of balanced sensing arms) exhibits better resolution. Nevertheless, both sensors have been able to detect the defected samples with the sparser density of defects (holes). Finally, the effects of device losses on the sensitivity have been qualitatively and quantitatively explained (see further details in Appendix A).

Appendix A

Let us consider sensor A (Fig. 4) by including the effects of losses in the step-impedance sensing line. Such losses can be accounted by means of a reflection coefficient seen from port 4 of the coupler satisfying $|\rho_{MUT}| < 1$. By contrast, the reflection coefficient seen from port 3 satisfies $|\rho_{REF}| = 1$, provided this port is left opened in sensor A. Under these conditions, the transmission coefficient (1) should be rewritten as

$$S_{21} = -\frac{1}{2}(\rho_{REF} - \rho_{MUT}) \approx -\frac{1}{2}(\mp 1 - |\rho_{MUT}|e^{j\phi_{MUT}}) \quad (A1)$$

The negative or positive sign of ρ_{REF} depends on whether the total number of high/low 90º line sections cascaded between the sensing line and the rat-race coupler, N, is even or odd, respectively. Note that for the device of Fig. 4, with a single section, i.e., $N = 1$, the sign should be positive, but for N even, the open-circuit at the extreme of the sensing line is seen as a short-circuit from port 4 of the coupler. Thus, for balancing purposes, ports 3 should also see a short-circuit, and thereby a negative sign in (A1) is required.

A variation in the dielectric constant of the MUT modifies the phase and the characteristic impedance of the sensing line, and this in turn affects the phase of the reflection coefficient, but also magnitude. Thus, the sensitivity by including the effects of losses in the sensing line cannot be merely expressed as (3). An additional term, that includes the influence of $|\rho_{MUT}|$ is needed. Thus, the sensitivity should be expressed as

$$S = \frac{d|S_{21}|}{d\varepsilon_{MUT}} = \frac{d|S_{21}|}{d\phi_{MUT}} \cdot \left\{ \frac{d\phi_{MUT}}{d\phi_{s,MUT}} \cdot \frac{d\phi_{s,MUT}}{d\varepsilon_{MUT}} + \frac{d\phi_{MUT}}{dZ_{s,MUT}} \cdot \frac{dZ_{s,MUT}}{d\varepsilon_{MUT}} \right\}$$
$$+ \frac{d|S_{21}|}{d|\rho_{MUT}|} \cdot \frac{d|\rho_{MUT}|}{d\varepsilon_{MUT}} \quad (A2)$$

Note, however, that the terms within the brackets ({}) are identical to those of (3), since ϕ_{REF}, $\phi_{s,REF}$, and $Z_{s,REF}$ are constant. Concerning the last term in (A2), for values of ε_{MUT} sufficiently distant from ε_{REF} (moderate and large perturbations), the losses at f_0 are negligible, and therefore the sensitivity is expected to be correctly predicted by expression (3). For small perturbations, the derivative $d|\rho_{MUT}|/d\varepsilon_{MUT}$ is expected to be close to zero, because when $\varepsilon_{MUT} = \varepsilon_{REF}$, $|\rho_{MUT}|$ is a minimum.

Let us next calculate the derivative $d|S_{21}|/d\phi_{MUT}$. The modulus of the transmission coefficient is simply

$$|S_{21}| = \frac{1}{2}\sqrt{1 \pm 2|\rho_{MUT}|\cos\phi_{MUT} + |\rho_{MUT}|^2} \quad (A3)$$

and (A3) coincides with (2) if $|\rho_{MUT}| = 1$ (lossless case), as expected. Thus, using (A3), the first derivative in (A2) is found to be

$$\frac{d|S_{21}|}{d\phi_{MUT}} = \frac{\mp|\rho_{MUT}| \cdot \sin\phi_{MUT}}{2\sqrt{1 \pm 2|\rho_{MUT}|\cos\phi_{MUT} + |\rho_{MUT}|^2}} \quad (A4)$$

If losses are absent ($|\rho_{MUT}| = 1$), (A4) is identical to (4), and the sensitivity in the limit of small perturbations ($\varepsilon_{MUT} = \varepsilon_{REF}$) is finite and given by expressions (10), (and, obviously, A4 is 1/2

in that limit, in coherence with expression 9). However, if losses are present ($|\rho_{MUT}| < 1$), the numerator of (A4) is null in the limit of small perturbations (where $\phi_{MUT} = 0$ for the case of N odd and $\phi_{MUT} = n\pi$ for the case of N even), whereas the denominator is finite in that limit. Therefore, $|S_{21}|/d\phi_{MUT} = 0$, and the overall sensitivity is null when $\varepsilon_{MUT} = \varepsilon_{REF}$, as it is verified in the text. This explains the dip in the sensitivity in the limit of small perturbations, as reported in the text (see Fig. 7 and related text). The dip is very narrow, and tends to disappear as losses decrease. Indeed, only a fine analysis in the vicinity of $\varepsilon_{MUT} = \varepsilon_{REF}$ is able to provide the data points necessary to capture this dip in the sensitivity inferred from the simulated data points, as discussed in the text. Nevertheless, it should be mentioned that as the sensitivity in the limit of small perturbations is enhanced, e.g., by including additional 90º line sections, the result is a narrowing effects in the sensitivity response. Thus, for sensing structures designed to exhibit extreme values of the sensitivity in the limit of small perturbations ($\varepsilon_{MUT} = \varepsilon_{REF}$), the prediction of the sensitivity given by the theory may be jeopardized by the effect of losses (since the interesting part of the sensitivity curve might be circumscribed to the range of ε_{MUT} affected by losses).

To illustrate the previous aspect, we have considered two additional structures, analyzed at simulation level. In both cases, the sensors are of type A, and the sensing arms consist of a high-impedance 90º sensing line, plus two cascaded 90º line sections with alternating low/high characteristic impedance ($N = 2$) in order to boost up the sensitivity in the limit of small perturbations. The difference is that in one case, the additional 90º line (the one in contact with the rat-race coupler) exhibits a high characteristic impedance of $Z_2 = 157$ Ω, whereas in the other sensing structure, such impedance is less extreme ($Z_2 = 70.71$ Ω). Apart from the addition of such high-impedance 90º line sections, the sensors under study are identical to the one of Fig. 4. Figure A1 depicts the absolute value of the sensitivity inferred from the simulated data points (by including the effects of losses) and the one predicted by the theory by excluding losses, corresponding to the sensor with $Z_2 = 70.71$ Ω. With this value of Z_2, the sensitivity in the limit of small perturbations ($\varepsilon_{MUT} \approx \varepsilon_{REF}$), as predicted by the lossless theory, is enhanced by a factor of 2, as compared to the one of the sensor of Fig. 4. Such value is also inferred by electromagnetic simulation (see Fig. A1). Indeed, except by the presence of the narrow dip, discussed before, the agreement between the theory and the simulated values of the sensitivity is excellent, similar to Fig. 7. Note, however, that the sensitivity response is narrower, as compared to Fig. 7, as predicted, and due to the enhanced sensitivity in the limit of small perturbations.

By contrast, for the sensing structure with $Z_2 = 157$ Ω, the expected sensitivity in the limit of small perturbations should be $|S| = 10.3$, according to the theoretical prediction by excluding losses. However, Fig. A2 reveals that the absolute value of the sensitivity inferred from the simulated data points does not coincide with the prediction of the theory by excluding losses, and the reason is the extremely peaked sensitivity response, as indicated. Thus, for extremely sensitive sensors, with very narrow sensitivity responses, the theory by excluding
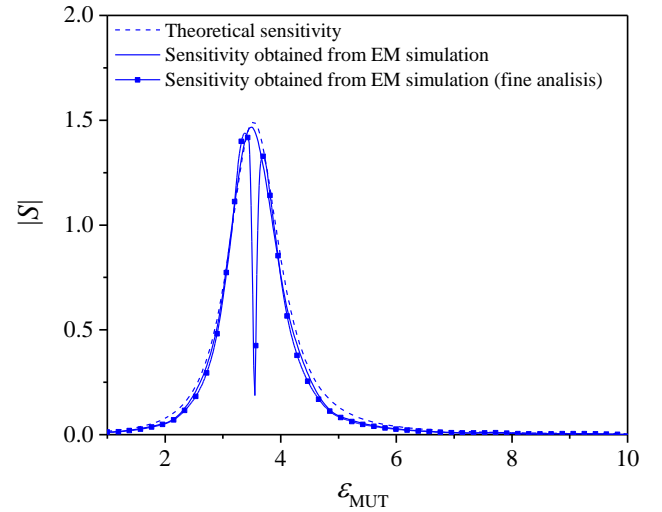

Fig. A1.   Sensor/comparator sensitivity corresponding to the device of Fig. 4 with an added 90º line section in the sensing arm with characteristic impedance $Z_2 = 70.71$ Ω.

losses (expression 3) overestimates the maximum sensitivity, due to the effect of losses. Nevertheless, it does not mean that by adding further 90º high/low impedance line sections to the sensing line the sensitivity cannot be enhanced. Indeed, Fig. A2 demonstrates that the maximum sensitivity (inferred from the simulated data points) is higher than in Fig. A1, but not as high as the theory (by excluding losses) predicts.

For an accurate prediction of the sensitivity in very high sensitive sensors, where the effects of losses cannot be circumvented, the use of expression (A2) is a due. However, the evaluation of the last derivative in (A2), i.e., $d|\rho_{MUT}|/\varepsilon_{MUT}$, entirely related to losses, is not simple, since the effects of losses depend on many factors. Therefore, the *a priori* determination of the sensitivity in highly sensitive sensors, where the effect of losses cannot be excluded, is not simple. Nevertheless, given a sensitive arm, with well-known substrate parameters and dimensions, it is possible to obtain the dependence of $|\rho_{MUT}|$ with ε_{MUT} at f_0 from electromagnetic simulation by including losses. From such dependence, evaluating the term $d|\rho_{MUT}|/\varepsilon_{MUT}$ is possible and, consequently, the sensitivity can be calculated. For that purpose, the other term contributing to the second summand of the sensitivity (A2), i.e., $d|S_{21}|/d|\rho_{MUT}|$, should also be calculated. Using (A3), such derivative is found to be

$$\frac{d|S_{21}|}{d|\rho_{MUT}|} = \frac{|\rho_{MUT}| \pm \cos\phi_{MUT}}{2\sqrt{1 \pm 2|\rho_{MUT}|\cos\phi_{MUT} + |\rho_{MUT}|^2}} \quad (A5)$$

and (A5) can be determined from the simulated reflection coefficient of the sensing arm, $\rho_{MUT} = |\rho_{MUT}|e^{j\phi_{MUT}}$, for the different values of the dielectric constant of the MUT. Nevertheless, it should be emphasized that this method requires the previous simulation of the reflection coefficient of the sensitive arm at f_0 as a function of the dielectric constant of the MUT. Fig. A2 also includes the sensitivity by including the effects of losses, i.e., inferred by means of (A2) according to the explained procedure, and the result is in good agreement with the simulated sensitivity. Therefore, these results point out that for moderate values of the sensitivity, the effects of losses can be ignored, and the sensitivity is correctly predicted by the
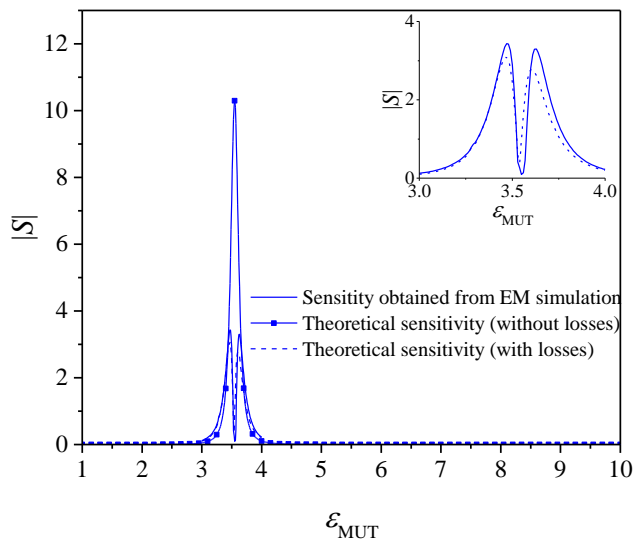
Fig. A2. Sensor/comparator sensitivity corresponding to the device of Fig. 4 with an added 90º line section in the sensing arm with characteristic impedance $Z_2 = 157\Omega$.

lossless theoretical expression. By contrast, when the sensitivity is high, the lossless expression overestimates the sensitivity. However, although more cumbersome, it is possible to calculate the sensitivity by including the effects of losses, provided the simulation of the reflection coefficient of the sensing arm for different values of the dielectric constant of the MUT is previously simulated. For that purpose, expression (A2), rather than expression (3) must be used.

It should be mentioned that in the previous analysis, we have not differentiated whether losses are due to the substrate or to the MUT sample. Nevertheless, the proposed sensors are devoted to the detection of defects in samples by comparison, rather than to the determination of the dielectric constant and loss tangent of the MUT samples.

REFERENCES

[1] M. Puentes, C. Weiß, M. Schüßler, and R. Jakoby, "Sensor array based on split ring resonators for analysis of organic tissues," in *IEEE MTT-S Int. Microw. Symp.*, Baltimore, MD, USA, Jun. 2011, pp. 1−4.

[2] A. Ebrahimi, W. Withayachumnankul, S. Al-Sarawi, and D. Abbott, "High-sensitivity metamaterial-inspired sensor for microfluidic dielectric characterization," *IEEE Sensors J.*, vol. 14, no. 5, pp. 1345−1351, May 2014.

[3] M. Schüßler, C. Mandel, M. Puentes, and R. Jakoby, "Metamaterial inspired microwave sensors," *IEEE Microw. Mag.*, vol. 13, no. 2, pp. 57–68, Mar. 2012.

[4] M. S. Boybay and O. M. Ramahi, "Material characterization using complementary split-ring resonators," *IEEE Trans. Instrum. Meas.*, vol. 61, no. 11, pp. 3039−3046, Nov. 2012.

[5] C.-S. Lee and C.-L. Yang, "Complementary split-ring resonators for measuring dielectric constants and loss tangents," *IEEE Microw. Wireless Compon. Lett.*, vol. 24, no. 8, pp. 563−565, Aug. 2014.

[6] C.-L. Yang, C.-S. Lee, K.-W. Chen, and K.-Z. Chen, "Noncontact measurement of complex permittivity and thickness by using planar resonators," *IEEE Trans. Microw. Theory Techn.*, vol. 64, no.1, pp. 247−257, Jan. 2016.

[7] L. Su, J. Mata-Contreras, P. Vélez, and F. Martín, "Estimation of the complex permittivity of liquids by means of complementary split ring resonator (CSRR) loaded transmission lines," in *2017 IEEE MTT-S International Microwave Workshop Series on Advanced Materials and Processes* (IMWS-AMP 2017), Pavia, Italy, 20-22 Sep. 2017.

[8] L. Su, J. Mata-Contreras, P. Vélez, A. Fernández-Prieto, and F. Martín, "Analytical method to estimate the complex permittivity of oil Samples," *Sensors*, 18(4), paper 984, 2018.

[9] A.K, Jha, N, Delmonte, A, Lamecki, M, Mrozowski, and M, Bozzi, "Design of microwave-based angular displacement sensor," *IEEE Microw. Wireless Compon. Lett.*, vol. 29 (4), pp. 306-308, Apr. 2019.

[10] G. Galindo-Romera, F. J. Herraiz-Martínez, M. Gil, J. J. Martínez-Martínez, and D. Segovia-Vargas, "Submersible printed split-ring resonator-based sensor for thin-film detection and permittivity characterization," *IEEE Sensors J.*, vol. 16, no. 10, pp. 3587-3596, May, 2016.

[11] R. A. Alahnomi, Z. Zakaria, E. Ruslan, S. R. A. Rashid, and A. A. M. Bahar, "High-Q sensor based on symmetrical split ring resonator with spurlines for solids material detection," *IEEE Sens. J.*., vol. 17, no. 9, pp. 2766-2775, May 2017.

[12] N. Jankovic and V. Radonic "A Microwave Microfluidic Sensor Based on a Dual-Mode Resonator for Dual-Sensing Applications," *Sensors*, vol. 17(12), p. 2713, 2017.

[13] H. Zhou, D. Hu, C. Yang, C. Chen, J. Ji, M. Chen, Y. Chen, Y. Chen, Y. Yang, and X. Mu, "Multi-Band Sensing for Dielectric Property of Chemicals Using Metamaterial Integrated Microfluidic Sensor," *Sci. Rep.*, vol. 8, paper 14801, 2018.

[14] M. A. H. Ansari, A. K. Jha, Z. Akhter, and M. J. Akhtar, "Multi-band RF planar sensor using complementary split ring resonator for testing of dielectric materials," *IEEE Sensors J.*, vol. 18, no. 16, pp. 6596-6606, Aug. 2018.

[15] M. Abdolrazzaghi, M. Daneshmand and A. K. Iyer, "Strongly Enhanced Sensitivity in Planar Microwave Sensors Based on Metamaterial Coupling," *IEEE Trans. Microw. Theory Techn.*, vol. 66, no. 4, pp. 1843-1855, Apr. 2018.

[16] K. Xu, *et al.*, "Novel Microwave Sensors Based on Split Ring Resonators for Measuring Permittivity", *IEEE Acesss*, vol. 6, pp. 26111-26120, 2018.

[17] H. Lobato-Morales, J. H. Choi, H. Lee, and J. L. Medina-Monroy, "Compact dielectric-permittivity sensors of liquid samples based on substrate-integrated-waveguide with negative-order-resonance," *IEEE Sensors J.*, vol. 19, no. 19, pp. 8694-8699, Oct. 2019.

[18] Y. Khanna and Y.K Awasthi, "Dual-band microwave sensor for investigation of liquid impurity concentration using a metamaterial complementary split-ring resonator," *J. Elect. Mat.*, vol 49, pp. 385–394, 2020.

[19] S. Mohammadi *et al.*, "Gold Coplanar Waveguide Resonator Integrated With a Microfluidic Channel for Aqueous Dielectric Detection," *IEEE Sensors J.*, vol. 20, no. 17, pp. 9825-9833, Sep. 2020.

[20] M. Abdolrazzaghi and M. Daneshmand, "Exploiting Sensitivity Enhancement in Micro-wave Planar Sensors Using Intermodulation Products with Phase Noise Analysis," *IEEE Trans. Circ. Syst. I: Reg. Papers*, vol. 67, no. 12, pp. 4382-4395, Dec. 2020.

[21] P. Vélez, J. Muñoz-Enano, A. Ebrahimi, C. Herrojo, F. Paredes, J. Scott, K. Ghorbani, and F. Martín, "Single-Frequency Amplitude-Modulation Sensor for Dielectric Characterization of Solids and Microfluidics", *IEEE Sensors J.*, vol. 21, no. 10, pp. 12189-12201, May 2021.

[22] C. Damm, M. Schussler, M. Puentes, H. Maune, M. Maasch, and R. Jakoby, "Artificial transmission lines for high sensitive microwave sensors," in *IEEE Sensors Conf.*, Christchurch, New Zealand, pp.755−758, Oct. 2009.

[23] F. J. Ferrández-Pastor, J. M. García-Chamizo, and M. Nieto-Hidalgo, "Electromagnetic differential measuring method: application in microstrip sensors developing," *Sensors*, vol. 17, p. 1650, 2017.

[24] M. Gil, P. Vélez, F. Aznar-Ballesta, J. Muñoz-Enano, and F. Martín, "Differential sensor based on electro-inductive wave (EIW) transmission lines for dielectric constant measurements and defect detection," *IEEE Trans. Ant. Propag.*, vol. 68, no. 3, pp. 1876-1886, Mar. 2020.

[25] J. Muñoz-Enano, P. Vélez, M. Gil, and F. Martín, "An analytical method to implement high sensitivity transmission line differential sensors for dielectric constant measurements," *IEEE Sensors J.*, vol. 20, pp. 178-184, Jan. 2020.

[26] J. Muñoz-Enano, P. Vélez, L. Su, M. Gil, P. Casacuberta, and F. Martín, "On the sensitivity of reflective-mode phase-variation sensors based on open-ended stepped-impedance transmission lines: theoretical analysis and experimental validation," *IEEE Trans. Microw. Theory Techn.*, vol. 69, no. 1, pp. 308-324, Jan. 2021.

[27] J. Muñoz-Enano, P. Casacuberta, L. Su, P. Vélez, M. Gil and F. Martín, "Open-Ended-Line Reflective-Mode Phase-Variation Sensors for Dielectric Constant Measurements", *IEEE Sensors 2020*, Rotterdam, The Netherlands, 25-28 Oct. 2020.

[28] L. Su, J. Muñoz-Enano, P. Vélez, P. Casacuberta, M. Gil, and F. Martín, "Highly sensitive phase variation sensors based on step-impedance coplanar waveguide (CPW) transmission lines," *IEEE Sensors J.*, vol. 21, no. 3, pp. 2864-2872, Feb. 2021.

[29] P. Casacuberta, J. Muñoz-Enano, P. Vélez, L. Su, M. Gil, and F. Martín, "Highly sensitive reflective-mode detectors and dielectric constant sensors based on open-ended stepped-impedance transmission lines," *Sensors*, vol. 20, paper 6236, 2020.

[30] J. Coromina, J. Muñoz-Enano, P. Vélez, A. Ebrahimi, J. Scott, K. Ghorbani, and F. Martín, "Capacitively-loaded slow-wave transmission lines for sensitivity improvement in phase-variation permittivity sensors," in *50th European Microwave Conference*, Utrecht, The Netherlands, Sep. 2020 (held virtually in Jan. 2021).

[31] L. Su, J Muñoz-Enano, P. Vélez, M. Gil, P. Casacuberta, and F. Martín, "Highly sensitive reflective-mode phase-variation permittivity sensor based on a coplanar waveguide (CPW) terminated with an open complementary split ring resonator (OCSRR)", *IEEE Access*, vol. 9, pp. 27928-27944, 2021.

[32] A. Ebrahimi, J. Coromina, J. Muñoz-Enano, P. Vélez, J. Scott, K. Ghorbani, and F. Martín, "Highly sensitive phase-variation dielectric constant sensor based on a capacitively-loaded slow-wave transmission line," *IEEE Trans. Circ. Systems I.*, vol. 68, no.7, pp. 2787-2799, Jul. 2021.

[33] L. Su, J. Naqui, J. Mata-Contreras and F. Martín, "Modeling Metamaterial Transmission Lines Loaded With Pairs of Coupled Split-Ring Resonators," *IEEE Ant. Wireless Propag. Lett.*, vol. 14, pp. 68-71, 2015.

[34] L. Su, J. Naqui, J. Mata-Contreras, F. Martín, "Modeling and applications of metamaterial transmission lines loaded with pairs of coupled complementary split ring resonators (CSRRs)", *IEEE Ant. Wireless Propag. Lett.*, vol. 15, pp. 154-157, 2016.

[35] J. Naqui, C. Damm, A. Wiens, R. Jakoby, Lijuan Su and F. Martín, "Transmission lines loaded with pairs of magnetically coupled stepped impedance resonators (SIRs): Modeling and application to microwave sensors," *2014 IEEE MTT-S Int. Microw. Symp.* (IMS2014), Tampa, FL, 2014, pp. 1-4.

[36] J. Naqui, C. Damm, A. Wiens, R. Jakoby, L. Su, J. Mata-Contreras, and F. Martín, "Transmission Lines Loaded With Pairs of Stepped Impedance Resonators: Modeling and Application to Differential Permittivity Measurements," *IEEE Trans. Microwave Theory Techn.*, vol. 64, no. 11, pp. 3864-3877, Nov. 2016.

[37] L. Su, J. Mata-Contreras, J. Naqui, and F. Martín, "Splitter/combiner microstrip sections loaded with pairs of complementary split ring resonators (CSRRs): modeling and optimization for differential sensing applications", *IEEE Trans. Microw. Theory Techn.*, vol. 64(12), pp. 4362-4370, Dec. 2016.

[38] L. Su, J. Mata-Contreras, and F. Martín, "Configurations of Splitter/Combiner Microstrip Sections Loaded with Stepped Impedance Resonators (SIRs) for Sensing Applications", *Sensors*, vol. 16(12), paper 2195, 2016.

[39] M.H. Zarifi, S. Farsinezhad, B.D. Wiltshire, M. Abdorrazaghi, N. Mahdi, P. Kar, M. Daneshmand, and K. Shankar, "Effect of phosphonate monolayer adsorbate on the microwave photoresponse of TiO2 nanotube membranes mounted on a planar double ring resonator", *Nanotechnology*, vol. 27, paper 375201, Sep. 2016.

[40] L. Su, J. Naqui, J. Mata-Contreras, F. Martín, "Cascaded Splitter/Combiner Microstrip Sections Loaded with Complementary Split Ring Resonators (CSRRs): Modeling, Analysis and Applications", *IEEE MTT-S Int. Microw. Symp.* (IMS'16), San Francisco, May 2016.

[41] P. Vélez, L. Su, K. Grenier, J. Mata-Contreras, D. Dubuc, and F. Martín, "Microwave microfluidic sensor based on a microstrip splitter/combiner configuration and split ring resonators (SRR) for dielectric characterization of liquids", *IEEE Sensors J.*, vol. 17, pp. 6589-6598, Oct. 2017.

[42] A. Ebrahimi, G. Beziuk, J. Scott, and K. Ghorbani, "Microwave Differential Frequency Splitting Sensor Using Magnetic-LC Resonators", *Sensors*, vol. 20, p. 1066, 2020.

[43] A. Ebrahimi, J. Scott, and K. Ghorbani, "Differential Sensors Using Microstrip Lines Loaded With Two Split-Ring Resonators", *IEEE Sens. J.*, vol. 18, pp. 5786–5793, 2018.

[44] J. Muñoz-Enano, P. Vélez, M. Gil, J. Mata-Contreras, and F. Martín, "Differential-mode to common-mode conversion detector based on rat-race couplers: analysis and application to microwave sensors and comparators," *IEEE Trans. Microw. Theory Techn.*, vol. 68, pp. 1312-1325, Apr. 2020.

[45] J. Muñoz-Enano, P. Vélez, M. Gil, and F. Martín, "Planar microwave resonant sensors: a review and recent developments", *Appl. Sci.*, vol. 10, p. 2615 (29 pages), 2020; doi:10.3390/app10072615.

[46] P. Vélez, J. Mata-Contreras, L. Su, D. Dubuc, K. Grenier, and F. Martín, "Modeling and analysis of pairs of open complementary split ring resonators (OCSRRs) for differential permittivity sensing," in *2017 IEEE MTT-S International Microwave Workshop Series on Advanced Materials and Processes* (IMWS-AMP 2017), Pavia, Italy, 20-22 September 2017.

[47] P. Vélez, K. Grenier, J. Mata-Contreras, D. Dubuc, and F. Martín, "Highly-sensitive microwave sensors based on open complementary split ring resonators (OCSRRs) for dielectric characterization and solute concentration measurement in liquids," *IEEE Access*, vol. 6, pp. 48324-48338, Aug. 2018.

[48] A. Ebrahimi, J. Scott, and K. Ghorbani, "Transmission lines terminated with LC resonators for differential permittivity sensing," *IEEE Microw. Wireless Compon. Lett.*, vol. 28(12), pp. 1149-1151, Dec. 2018.

[49] P. Vélez, J. Muñoz-Enano, K. Grenier, J. Mata-Contreras, D. Dubuc, and F. Martín, "Split ring resonator (SRR) based microwave fluidic sensor for electrolyte concentration measurements," *IEEE Sensors J.*, vol. 19, no. 7, pp. 2562-2569, Apr. 2019.

[50] P. Vélez, J. Muñoz-Enano, M. Gil, J. Mata-Contreras, and F. Martín, "Differential microfluidic sensors based on dumbbell-shaped defect ground structures in microstrip technology: analysis, optimization, and applications," *Sensors*, vol. 19, page 3189, 2019.

[51] P. Vélez, J. Muñoz-Enano, and F. Martín, "Differential sensing based on quasi-microstrip-mode to slot-mode conversion," *IEEE Microw. Wireless Compon. Lett.*, vol. 29, pp. 690-692, Oct. 2019.

[52] J. Muñoz-Enano, P. Vélez, M. Gil, and F. Martín, "Microfluidic reflective-mode differential sensor based on open split ring resonators (OSRRs)," *Int. J. Microw. Wireless Technol*, vol. 12, pp. 588-597, Sep. 2020.

[53] J. Muñoz-Enano, P. Vélez, M. Gil, E. J. Cunilleras, A. Bassols, and F. Martín, "Characterization of electrolyte content in urine samples through a differential microfluidic sensor based on dumbbell-shaped defect ground structures," *Int. J. Microw. Wireless Technol.*, vol. 12(9), pp. 817-824, Sep. 2020.

[54] A. Ebrahimi, F. J. Tovar-Lopez, J. Scott, and K. Ghorbani, "Differential microwave sensor for characterization of glycerol–water solutions," *Sens. & Act. B: Chem.*, vol. 321, Art. no. 128561, 2020.

[55] J. Mata-Contreras, C. Herrojo, and F. Martín, "Application of split ring resonator (SRR) loaded transmission lines to the design of angular displacement and velocity sensors for space applications", *IEEE Trans. Microw. Theory Techn.*, vol. 65, no. 11, pp. 4450-4460, Nov. 2017.

[56] C. Herrojo, F. Paredes, and F. Martín "Synchronism and Direction Detection in High-Resolution/High-Density Electromagnetic Encoders", *IEEE Sensors J.*, vol. 21, no. 3, pp. 2873-2882, Feb. 2021.

[57] D.M. Pozar, *Microwave Engineering*, 4th Ed., John Wiley, Hoboken, NJ, USA, 2011.

[58] A. Lai, T. Itoh and C. Caloz, "Composite right/left-handed transmission line metamaterials," *IEEE Microwave Magazine*, vol. 5, no. 3, pp. 34-50, Sep. 2004.

[59] M. Beruete, F. Falcone, M. J. Freire, R. Marqués, and J. D. Baena, "Electroinductive waves in chains of complementary metamaterial elements," *Appl. Phys. Lett.*, vol. 88, Art. no. 083503, Jan. 2006.

[60] L. Su, J. Muñoz-Enano, P. Vélez, P. Casacuberta, M. Gil, F. Martín, "Phase-Variation Microwave Sensor for Permittivity Measurements Based on a High-Impedance Half-Wavelength Transmission Line", *IEEE Sensors J.*, vol. 21, no. 9, pp. 10647-10656, May 2021.
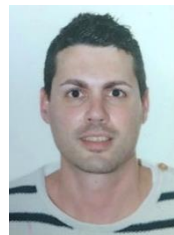
C. Herrojo was born in Barcelona, Spain, in 1983. He received the Telecommunications Technical Engineering degree in electronic systems and Telecommunications Engineering degree from the Universitat Autònoma de Barcelona in 2010 and 2012, respectively and the PhD degree in Electronics Engineering from the same university in 2018. His research interests include RF/microwave devices, Chipless-RFID and RFID technology, and Metamaterials.

Paris Vélez (S'10–M'14–SM'21) was born in Barcelona, Spain, in 1982. He received the degree in Telecommunications Engineering, specializing in electronics, the Electronics Engineering degree, and the Ph.D. degree in Electrical Engineering from the Universitat Autònoma de Barcelona, Barcelona, in 2008, 2010, and 2014, respectively. His Ph.D. thesis concerned common mode suppression differential microwave circuits based on metamaterial concepts and semi-lumped resonators. During the Ph.D., he was awarded with a pre-doctoral teaching and research fellowship by the Spanish Government from 2011 to 2014. From 2015-2017, he was involved in the subjects related to metamaterials sensors for fluidics detection and characterization at LAAS-CNRS through a TECNIOSpring fellowship cofounded by the Marie Curie program. From 2018 to 2020 he has worked in miniaturization of passive circuits RF/microwave and sensors-based metamaterials through Juan de la Cierva fellowship. His current research interests include the miniaturization of passive circuits RF/microwave and sensors-based metamaterials. Dr. Vélez is a Reviewer for the IEEE Transactions on Microwave Theory and Techniques and for other journals.

Jonathan Muñoz-Enano was born in Mollet del Vallès (Barcelona), Spain, in 1994. He received the Bachelor's Degree in Electronic Telecommunications Engineering in 2016 and the Master's Degree in Telecommunications Engineering in 2018, both at the Autonomous University of Barcelona (UAB). Actually, he is working in the same university in the elaboration of his PhD, which is focused on the development of microwave sensors based on metamaterials concepts for the dielectric characterization of materials and biosensors.

Lijuan Su was born in Qianjiang (Hubei), China in 1983. She received the B.S. degree in communication engineering and the M.S. degree in circuits and systems both from Wuhan University of Technology, Wuhan, China, in 2005 and 2013 respectively, and the Ph.D. degree in electronic engineering from Universitat Autonoma de Barcelona, Barcelona, Spain, in 2017. From Nov. 2017 to Dec. 2019, she worked as a postdoc researcher in Flexible Electronics Research Center, Huazhong University of Science and Technology, Wuhan, China. She is currently a postdoc researcher in CIMITEC, Universitat Autonoma de Barcelona, Spain. Her current research interests focus on the development of novel microwave sensors with improved performance for biosensors, dielectric characterization of solids and liquids, defect detection, industrial processes, etc.

Pau Casacuberta was born in Sabadell (Barcelona), Spain, in 1997. He received the Bachelor's Degree in Electronic Telecommunications Engineering and the Bachelor's Degree in Computer Engineering in 2020, both from the Universitat Autònoma de Barcelona (UAB). Currently, he is in his junior year of the Master's Degree in Telecommunications Engineering in the UAB. He received the Collaboration fellowship by the Spanish Government in 2019 for developing his Bachelor's Thesis in highly sensitive microwave sensors based in stepped impedance structures.

Marta Gil Marta Gil (S'05-M'09) was born in Valdepeñas, Ciudad Real, Spain, in 1981. She received the Physics degree from Universidad de Granada, Spain, in 2005, and the Ph.D. degree in electronic engineering from the Universitat Autònoma de Barcelona, Barcelona, Spain, in 2009. She studied one year with the Friedrich Schiller Universität Jena, Jena, Germany. During her PhD Thesis she was holder of a METAMORPHOSE NoE grant and National Research Fellowship from the FPU Program of the Education and Science Spanish Ministry. As a postdoctoral researcher, she was awarded with a Juan de la Cierva fellowship working in the Universidad de Castilla-La Mancha. She was postdoctoral researcher in the Institut für Mikrowellentechnik und Photonik in Technische Universität Darmstadt and in the Carlos III University of Madrid. She is currently associate professor in the Universidad Politécnica de Madrid within the Excellence Program for University Professoriat of the V Regional Plan for Scientific Research and Technological Innovation of the Administration of the Community of Madrid. She has worked in metamaterials, piezoelectric MEMS and microwave passive devices. Her current interests include metamaterials sensors for fluidic detection

Ferran Martín (M'04-SM'08-F'12) was born in Barakaldo (Vizcaya), Spain in 1965. He received the B.S. Degree in Physics from the Universitat Autònoma de Barcelona (UAB) in 1988 and the PhD degree in 1992. From 1994 up to 2006 he was Associate Professor in Electronics at the Departament d'Enginyeria Electrònica (Universitat Autònoma de Barcelona), and since 2007 he is Full Professor of Electronics. In recent years, he has been involved in different research activities including modelling and simulation of electron devices for high frequency applications, millimeter wave and THz generation systems, and the application of electromagnetic bandgaps to microwave and millimeter wave circuits. He is now very active in the field of metamaterials and their application to the miniaturization and optimization of microwave circuits and antennas. Other topics of interest include microwave sensors and RFID systems, with special emphasis on the development of high data capacity chipless-RFID tags. He is the head of the Microwave Engineering, Metamaterials and Antennas Group (GEMMA Group) at UAB, and director of CIMITEC, a research Center on Metamaterials supported by TECNIO (Generalitat de Catalunya). He has organized several international events related to metamaterials and related topics, including Workshops at the IEEE International Microwave Symposium (years 2005 and 2007) and European Microwave Conference (2009, 2015 and 2017), and the Fifth International Congress on Advanced Electromagnetic Materials in Microwaves and Optics (Metamaterials 2011), where he acted as Chair of the Local Organizing Committee. He has acted as Guest Editor for six Special Issues on metamaterials and sensors in five International Journals. He has authored and co-authored over 650 technical conference, letter, journal papers and book chapters, he is co-author of the book on Metamaterials entitled Metamaterials with Negative Parameters: Theory, Design and Microwave Applications (John Wiley & Sons Inc.), author of the book Artificial Transmission Lines for RF and Microwave Applications (John Wiley & Sons Inc.), co-editor of the book Balanced Microwave Filters (Wiley/IEEE Press) and co-author of the book Time-Domain Signature Barcodes for Chipless-RFID and Sensing Applications (Springer). Ferran Martín has generated 21 PhDs, has filed several patents on metamaterials and has headed several Development Contracts.

Prof. Martín is a member of the IEEE Microwave Theory and Techniques Society (IEEE MTT-S). He is reviewer of the IEEE Transactions on Microwave Theory and Techniques and IEEE Microwave and Wireless Components Letters, among many other journals, and he serves as member of the Editorial Board of IET Microwaves, Antennas and Propagation, International Journal of RF and Microwave Computer-Aided Engineering, and Sensors. He is also a member of the Technical Committees of the European Microwave Conference (EuMC) and International Congress on Advanced Electromagnetic Materials in Microwaves and Optics (Metamaterials). Among his distinctions, Ferran Martín has received the 2006 Duran Farell Prize for Technological Research, he holds the Parc de Recerca UAB – Santander Technology Transfer Chair, and he has been the recipient of three ICREA ACADEMIA Awards (calls 2008, 2013 and 2018). He is Fellow of the IEEE and Fellow of the IET.